IOP PUBLISHING JOURNAL OF MICROMECHANICS AND MICROENGINEERING

J. Micromech. Microeng. **20** (2010) 015039 (8pp) doi:10.1088/0960-1317/20/1/015039

On the use of shape memory alloy thin films to tune the dynamic response of micro-cantilevers

T Kniknie[1], Y Bellouard[1,3], E Homburg[1], H Nijmeijer[1], X Wang[2] and J J Vlassak[2]

[1] Mechanical Engineering Department, Eindhoven University of Technology, Eindhoven, The Netherlands
[2] SEAS, Harvard University, Cambridge, MA, USA

E-mail: y.bellouard@tue.nl

Received 9 September 2009, in final form 16 October 2009
Published 14 December 2009
Online at stacks.iop.org/JMM/20/015039

Abstract
We investigate the effect of martensitic phase transformations on the dynamic response of commercial AFM silicon cantilevers coated with shape memory alloy (SMA) thin films. We propose a simple thermo-mechanical model to predict the phase transformation. We show experimentally that the SMA thin film dynamic response can be actively changed upon heating and cooling. This can be used for vibration control in micro-systems.

(Some figures in this article are in colour only in the electronic version)

1. Introduction

Initially developed for scanning probe microscopy (AFM, STM) [1] micro-cantilevers are now used in a large number of applications, for instance mass sensing [2], gas and biological sensors [3], and new concepts of memory (the Millipede® from IBM) that features an array of cantilevers [4]. To improve the performance of sensing micro-cantilever-based devices and to further extend the potential applications of cantilevers, control of the dynamical behaviour of the beam is of particular interest, for instance, to reject unwanted vibrations in sensors applications, to increase the positioning accuracy in actuators applications, or to simply broaden the measurement range for sensing applications.

In this paper, we focus on demonstrating the use of a shape memory alloy (SMA) thin film to actively change the dynamic response of AFM cantilevers. More specifically, we show that an electrical current can effectively be used to modify the frequency response of AFM cantilevers coated with SMA.

Shape memory alloys show temperature- and stress-induced thermoelastic phase transformations between two (or more) solid-state phases [8] that lead to the well-known shape memory effect and the so-called superelastic effect. In addition, shape memory alloys also exhibit variable damping properties during the transformation as well as a dramatic change of Young's modulus. The latter can be used to actively control the dynamical response of a mechanical structure.

The use of SMA for tuneable damping and frequency response has been investigated for various applications such as buildings with earthquake protection [5], skis [7], aircraft [6] and flexures [9]. Further, SMA are attractive for microsystems in particular due to their high-work density and the possibility of using SMA thin films. A review of applications of SMA in micro-systems is given in [10]. More specifically, the damping properties of SMA thin films have been reviewed by Wuttig *et al* [22].

In this study, we investigate the use of a SMA coating to actively modify the dynamical response of AFM cantilevers. As a first proof-of-concept, we report on the active control of resonant frequencies. In section 2, the experimental procedure and setup are described. There we investigate the quasi-static thermo-mechanical behaviour. In the following section, we report on the dynamical behaviour, and finally in section 4, we conclude on the potential use of SMA thin films to tune the dynamic response of microsystems.

[3] Author to whom any correspondence should be addressed.

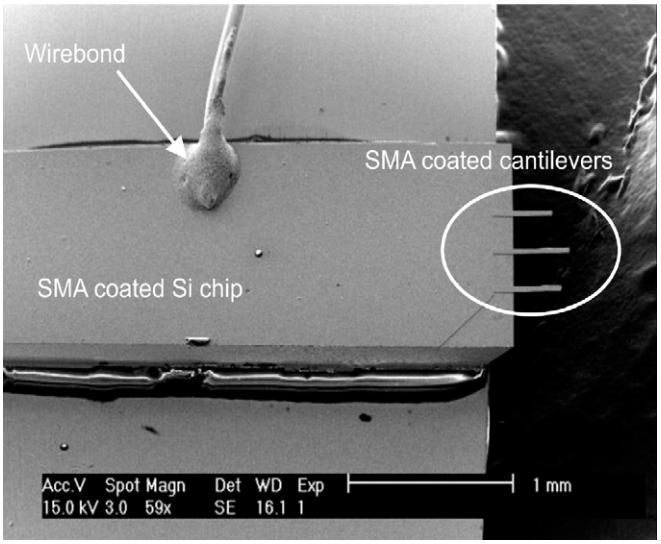

Figure 1. SEM picture of NiTi coated silicon micro cantilevers.

2. Quasi-static thermo-mechanical behaviour

2.1. Test specimens

We use commercially available tip-less silicon cantilevers (shown in figure 1) (Micro-Masch [18]). The cantilevers are coated with an equi-atomic NiTi thin film by means of magnetron sputtering. The lengths are 250 μm and 300 μm, width is 35 μm and the thickness is approximately 2 μm.

The NiTi thin film has a thickness h_f of $\sim$1 μm. Sputter deposition takes place at room temperature in a vacuum system with a base pressure of better than 5×10^{-8} Torr and an Ar working pressure of 1.5 mTorr. After deposition, the NiTi film is amorphous. Crystallization of the film takes place during an annealing step at 500 °C for 30 min [11].

The cantilevers are part of a silicon chip (l × w × h, 3.4 × 1.6 × 0.4 mm). This chip is mounted on a steel plate for easy handling and positioning. After sputtering and annealing, the cantilevers are bent up due to residual tensile stress present in the film.

2.2. Thermo-mechanical experiments and modelling

The phase transformation temperatures and the influence of the phase transitions on the mechanical behaviour of the system are investigated by measuring temperature–stress curves. The stress in the SMA film on a silicon cantilever is estimated using Timoshenko's equation for the maximum stress in bimetallic thermostats [18]:

$$\sigma = \frac{1}{\rho}\left[\frac{2}{(h_s+h_f)h_f}(E_sI_s+E_fI_f)+\frac{h_fE_f}{2}\right] \qquad (2.1)$$

with curvature $1/\rho$ (1/m), Young's modulus E and second moment of area I. For the silicon cantilever and SMA film, we use the indices s and f, respectively. The cantilever has a thickness h_s and the film a thickness h_f. In this equation, the stress is measured at the interface between the two materials.

Equation (2.1) shows that the stress inside the film can be estimated from beam curvature measurements. Therefore, we use the temperature–curvature graph to determine the phase transformation behaviour of the SMA and then, to compute the stress in the material.

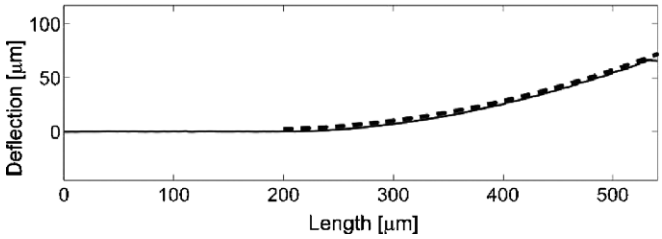

Figure 2. Deflection profile and curve fit of a coated cantilever with length $L = 350$ μm at room temperature. Using the polynomial of this fitted curve, the curvature of the cantilever is computed using equation (2.2).

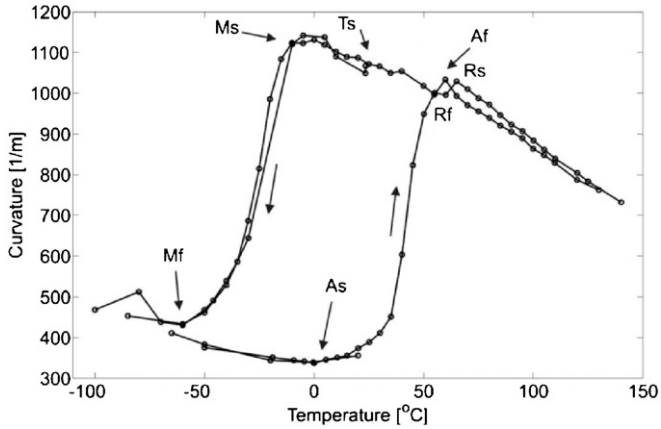

Figure 3. Temperature–curvature graph of a NiTi coated silicon micro cantilever with length $L = 250$ μm. Temperature is cycled between −100 °C and 140 °C with steps of 5 °C.

The deflection profile of the coated cantilever is measured for various temperatures starting from −100 °C and up to 150 °C. The profile is measured using a 3D optical profiler (Sensofar PLμ 2300) equipped with an accurate heating/cooling stage with a resolution of 0.1 °C. The profiler measures height information of the cantilever. The curvature of the cantilever is determined using the beam curvature equation (so-called Euler's 'Elastica') for various positions on the beam:

$$\frac{1}{\rho} = \frac{\frac{\partial^2 z}{\partial x^2}}{\left[1+\left(\frac{\partial z}{\partial x}\right)^2\right]^{3/2}}. \qquad (2.2)$$

Once ρ is known (using equation (2.2)), we calculate the stress in the film throughout the length of the beam (using equation (2.1)).

An example of such a deflection measurement is shown in figure 2. A polynomial curve fit is used to extract the beam curvature from the measurements.

The temperature–curvature graph of a cantilever with length 250 μm during a thermal cycle between −100 °C and 140 °C is shown in figure 3.

Going through a temperature cycle, some interesting observations can be made. First, the sample is cooled down from room temperature T_s = 23.5 °C to −100 °C.

Below $M_f = -56.6$ °C, the film is fully in the martensite phase (the low-temperature crystallographic phase of the material). Upon increasing the temperature, the cantilever bends down due to its bimorph structure. At $A_s = 1$ °C, the phase transformation from martensite to austenite (the high-temperature crystallographic phase of the material) starts. During the phase transformation, the cantilever bends up until the temperature reaches 63.4 °C. Above this temperature, noted as A_f, the material is fully transformed in the austenite phase. Further increasing the temperature again results in downward bending due to the bimorph effect. The slope of this part of the graph differs from the slope in the martensitic state because both thermal expansion coefficient and Young's modulus have changed during the phase transformation.

If the temperature is decreased, a reverse phase transformation takes place. During cooling, an intermediate phase appears. We identify this intermediate phase as the R-phase, an intermediate crystallographic phase observed during the reverse transformation from austenite to martensite in Ni–Ti binary alloys. Between $R_s = 58.6$ °C and $R_f = 49.0$ °C some small hysteresis effect is observed corresponding to the austenite to R-phase transformation. Below R_f, the material is in R-phase until the temperature reaches $M_s = -3.8$ °C where a second transformation, from R-phase to martensite takes place. During the transformation the cantilever bends downward.

Below the temperature M_f the material is fully in martensite phase and no more phase transformations are observed.

2.3. Discussion

Although the R-phase can be suppressed if the material is under tensile stress, the appearance of the R-phase in our case is explained by the fact that the stress levels in the film are relatively low [20]. The stress discontinuity and the different slope after transformation (between R_f and M_s) in figure 2 indicate that indeed a two-step transformation takes place. We also note that the width of the austenite–martensite hysteresis is almost 60 °C, which is rather large for an equi-atomic NiTi [21].

To compute the stress in the film, two important assumptions are made. First, we assume that the material properties remain constant for a given phase. Second, we state that during phase transformation, the thermal expansion coefficient and Young's modulus of the SMA film change linearly with temperature. We use selected material properties and the coated cantilever to estimate the stress in the film (see table 1 for details). Figure 4 shows the evolution of Young's modulus as a function of temperature.

The modulus for silicon is calculated taking into account the crystal orientation with respect to the cantilever orientation and the bending mode loading using the method described in [19].

In our model, we only consider the stress at the interface between the SMA film and the silicon cantilever for which equation (2.1) (from Timoshenko's paper) holds.

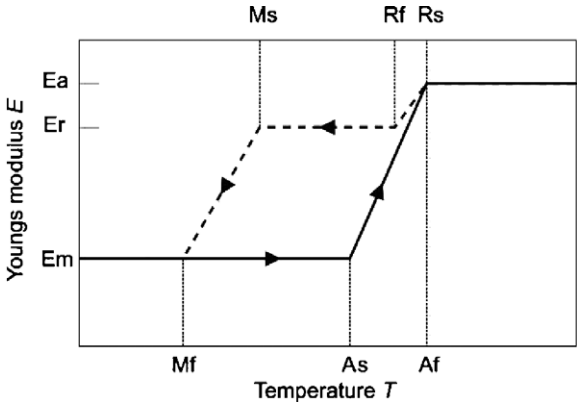

Figure 4. The evolution of Young's modulus of SMA during a temperature cycle. The austenite modulus E_a, martensite modulus E_m and R-phase modulus E_r are indicated, as well as the transformation temperatures.

Table 1. Material properties, dimensions and transformation temperatures of the SMA coated cantilever.

Mechanical properties (GPa)				
E_m	E_a	E_r	E_S	σ_0
30	80	70	130	0.026
Dimensions (μm)				
L	W	h_f	h_s	
348	35	1.2	1.7	
Thermal expansion coefficients (μm/m K^{-1})				
α_m	α_a	α_r	α_s	
6.6	11	7	2.6	
Transformation temperatures (°C)				
A_s	A_f	R_s	R_f	M_s	M_f	T_0
1.0	63.4	58.6	49	−3.8	−56.6	−70

Figure 5 shows the stress in the film deposited on a 250 μm long cantilever. From this figure we can clearly distinguish the three phases that occur in the film.

2.4. Modelling of the bimorph effect

To predict the SMA film stress as a function of temperature, a thermo-mechanical model is made. The film stress is subdivided into three elements:

$$\sigma = \sigma_0 + \sigma_b + \sigma_t \tag{2.3}$$

where σ_0 is the initial stress, σ_b is the bimorph stress and σ_t is the transformation stress. The initial stress σ_0 is determined at $T_0 = -70$ °C when the stress in the film is purely due to the thermal mismatch between the film and the cantilever. The cantilever has a positive curvature at this temperature.

The beam curvature can be decomposed into two terms. One represents the initial curvature due to the presence of residual stress from the sputtering/annealing steps. The second term indicates the bimorph effect observed while

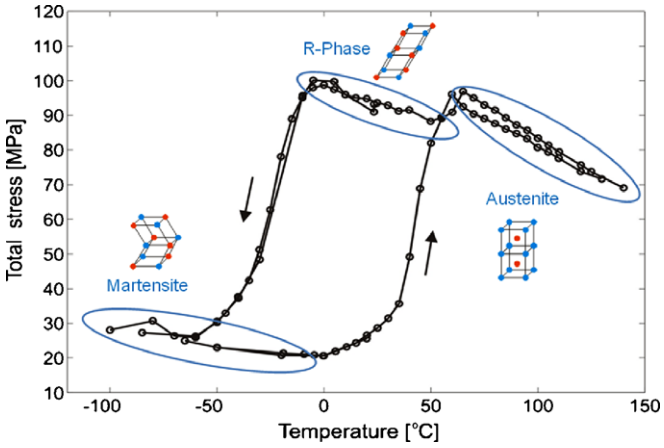

Figure 5. Temperature–stress graph of the NiTi coated silicon cantilever with length $L = 250$ um. The regions corresponding to fully transformed phases are indicated. Direction of the temperature cycle is indicated with arrows.

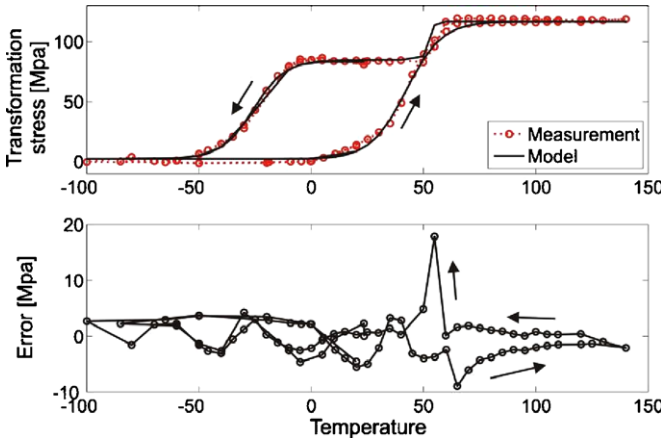

Figure 6. Transformation stress with the fitted hysteresis model.

changing the cantilever temperature. We use Timoshenko's equation [2.1] to describe these two terms:

$$\rho = \rho_0 + \frac{(\alpha_f - \alpha_s)(T - T_0)}{\frac{h_s+h_f}{2} + \frac{2(E_s I_s + E_f I_f)}{h_s+h_f}\left(\frac{1}{E_s h_s w} + \frac{1}{E_f h_f w}\right)} \tag{2.4}$$

where α_f and α_s are respectively the thermal expansion coefficient of the film and the cantilever, and w is the width of the cantilever. An initial curvature ρ_0 at $T = T_0$ models initial stress σ_0 in the film.

Subtracting the bimorph stress from the stress in figure 5 and taking into account the change of material properties as illustrated in figure 4, gives σ_t, the stress change due to phase transformations (see figure 6). In this temperature–stress curve, we observe that, while fully transformed in a given phase, the stress in the material does not change since the stress contribution resulting from the bimorph effect is suppressed.

2.5. Modelling of the phase transformation

The modelling of the phase transformations in SMA has been addressed by many authors in particular from the viewpoint of material science [12, 13], or from a purely mathematical approach [14]. More generally, the phenomenological modelling of hysteresis has been broadly addressed (see [17] for a review). Among these models, we choose the Krasnosel'skii–Pokrovskii [15] hysteron because of its appealing simplicity while it is still capable of capturing most of the geometrical properties of the hysteresis curve. The general formulation of the model is

$$\sigma(T) = \begin{cases} \max\{\sigma_{t,0}, \Gamma_+(T)\} & \text{when is } T \text{ non-decreasing} \\ \min\{\sigma_{t,0}, \Gamma_-(T)\} & \text{when is } T \text{ non-increasing.} \end{cases} \tag{2.5}$$

In this model, one is free to choose the functions Γ_+ and Γ_- to fit measured curves. Since the major loop shows a saturation behaviour in both the austenite–R-phase transformation and the R-phase–martensite transformation (the dead zones), it is quite natural to use saturation functions fitting the data. To model the major loop for increasing temperature, we use one sigmoidal function as fit and two superposed sigmoidal functions when the temperature decreases:

$$\begin{aligned} \Gamma_+ &= S(T, \bar{p}_1) \\ \Gamma_- &= S(T, \bar{p}_2) + S(T, \bar{p}_3) \\ S(T, \bar{p}_i) &= p_{i1} + p_{i2}(1 + \mathrm{e}^{p_{i3}}(T - p_{i4}))^{-1}. \end{aligned} \tag{2.6}$$

The function $S(T, p_i)$ requires four parameters p_{ii}, so the total model has 12 parameters to be determined from curve fitting with the measured data. We divide the major loop into three intervals where the sigmoidal functions are fitted

$$\begin{aligned} &S(T, \bar{p}_1) \quad \text{for} \quad \dot{T} > 0 \\ &S(T, \bar{p}_2) \quad \text{for} \quad \dot{T} < 0 \quad \text{and} \quad T < R_f \\ &S(T, \bar{p}_3) \quad \text{for} \quad \dot{T} < 0 \quad \text{and} \quad T < M_s. \end{aligned} \tag{2.7}$$

The results of the identification procedure are shown in figure 6. The error stays within 5%, except for the R-phase transitions, where the slope of the measured graph (model or data) changes abruptly.

In figure 6, the transformation stress has been extracted from the total measured stress in the cantilever. Comparing figures 5 and 6 illustrates the contributions of the two mechanisms, phase transformation and bimorph effect, and fully explains the thermo mechanical behaviour of the system.

3. Dynamic behaviour

To determine whether the phase transitions in the SMA significantly influence the dynamics of the cantilever, we perform a frequency domain analysis as a function of temperature. The location and the shape of the resonant peaks of the system are analysed to obtain information about stiffness and damping properties. To measure the cantilever dynamic's response, we designed a dedicated experimental setup described in the next subsection.

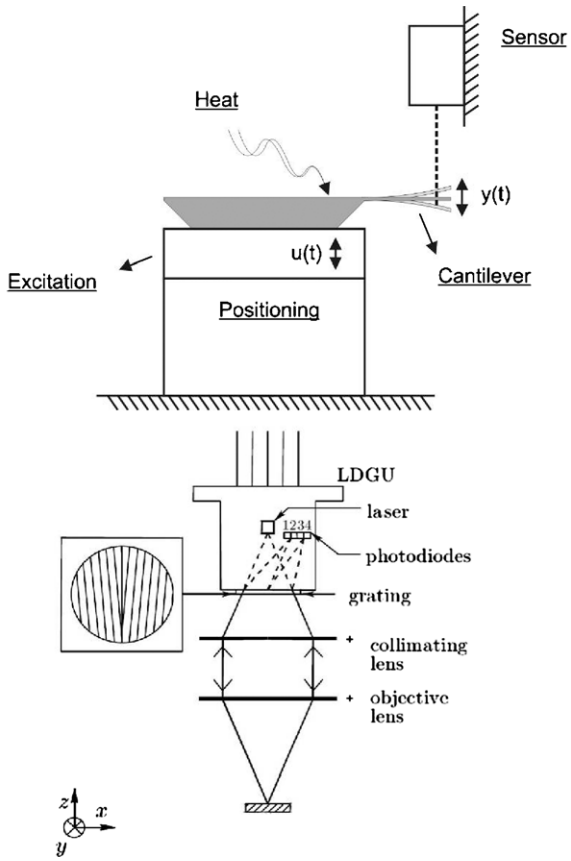

Figure 7. Schematic representation of the measurement setup (top) and a picture of the excitation and heating stage for dynamic measurements (bottom). Schematic representation of the optical measurement head, a laser detector grating unit (LDGU).

3.1. Experimental setup and procedure

The cantilevers are randomly excited by a piezoelectric element while the cantilever beams are heated by passing an electrical current through the SMA film. The tip vibrations are recorded by an optical measurement system (further described below) and compared to the input excitation. A schematic drawing of the measurement setup and a picture of the realized excitation and heating stage are shown in figure 7.

The steel plate on which the silicon chip with cantilevers is mounted is placed on a kinematic mount similar to those used in an AFM, and is coupled to the excitation stage by two neodymium magnets.

The optical measurement system is based on a laser detector grating unit (LDGU), schematically shown in figure 7. It consists of a laser, a diffraction grating, lenses and photodiodes. The system estimates how much the laser beam is out of focus from the measured surface, by subtracting and normalizing the diode signals. This technique has been extensively used for decades in compact-disc players. Although the measurement system is compact and simple, it provides an accurate way for measuring small displacement at high frequency.

We analyse the dynamic response of the cantilever as a function of the current passing through the SMA film. Ideally, it would be better to have a direct measurement

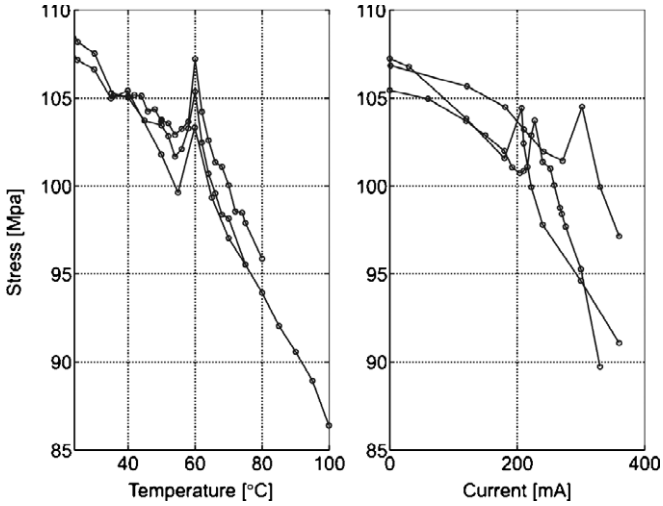

Figure 8. Calculated stress in the film as a function of temperature and current. The left graph is a detailed measurement of the stress–temperature behaviour, as explained in section 2.2 and shown in figure 5. The right graph shows the same experimental data but with resistive heating.

of the cantilever temperature; however, in practice this is very difficult to implement due to the size of the micro-devices. Rather, we choose to calibrate the current response with respect to temperature using a heating/cooling stage to modify the cantilever temperature in a controlled environment (figure 8). We observed a lack of repeatability in the current transformation curves (as can be seen in figure 8). This is due to some fluctuation in the contact resistance of the wire-bonds. (In our case, a four-point measurement (which would bypass this issue) could not be implemented due to technical difficulties and spatial constraints.) Nevertheless, the calibration curves illustrate quantitatively the direct relation between electrical current and temperature (as one may expect).

Starting at room temperature, the cantilever chip is excited with a random white noise signal. Two measurements of the dynamic response are recorded: the vibration amplitudes as a function of amplitude $H_{\text{fixed}}(\text{j}\omega)$ at the fixed end of the cantilever and $H_{\text{free}}(\text{j}\omega)$ at the free end. The frequency response function of the excitation signal to the dynamics of the cantilever is determined by dividing these two measurements:

$$H_{\text{cant}} = \frac{H_{\text{free}}}{H_{\text{fixed}}}. \tag{3.1}$$

This measurement is performed as a function of increasing current through the film, i.e. indirectly, as a function of increasing temperature.

3.2. Experimental results

The vibration amplitude is measured as a function of frequency and increasing current applied to the SMA film for several cantilever lengths. We show the results for a 250 μm cantilever in figure 10 and for a 350 μm cantilever in figure 11. For the 250 μm cantilever, the flexural resonance frequency is found around 37 kHz, as specified by the cantilever supplier. We use this value to estimate the frequency range of interest to

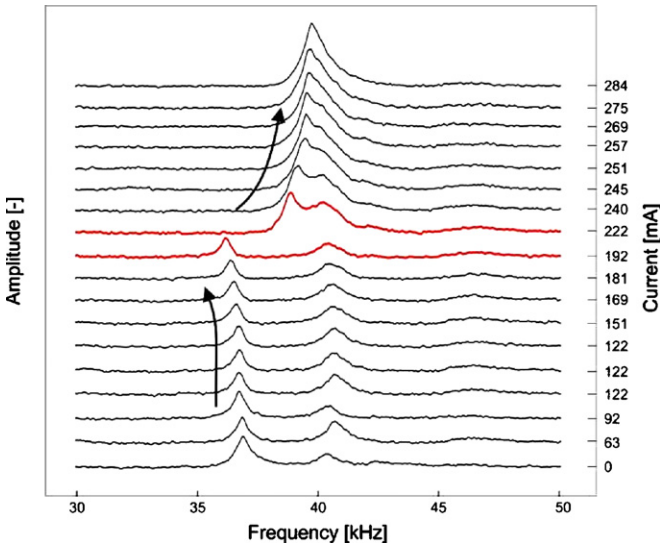

Figure 9. Frequency response functions of the NiTi coated cantilever with length $L = 250$ μm. The amplitude is recorded for increasing current, as indicated on the right-hand side axis. (The graphs related to a sharp transition are found for supplied current between 190 and 225 mA.)

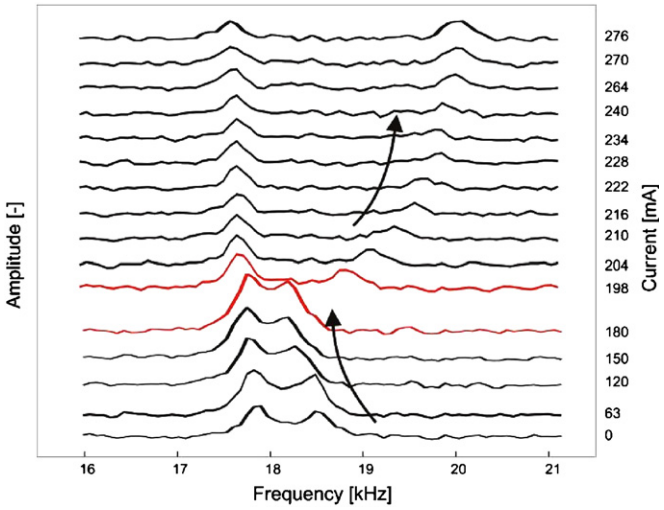

Figure 10. Frequency response functions of the NiTi coated cantilever with length $L = 350$ μm. The amplitude is recorded for increasing current, as indicated on the right-hand side axis. (The graphs related to a sharp transition are found for supplied current between 180 and 200 mA.)

analyse the flexural dynamics of the coated cantilever. (For the 350 μm cantilever, the frequency range of interest is estimated around 18 kHz.) Our setup only allows us to investigate the dynamics of the cantilever above room temperature. We start our experiments by heating up the cantilever so that the full austenite transformation occurs.

At low current levels, we see the first resonance peak in the figure decreasing for increasing currents (figure 9). The second peak around 41 kHz also decreases slightly. When the current is higher than 200 mA, a dramatic increase of the first resonance peak occurs while the second peak further decreases. Above a certain current threshold (about 200–210 mA in figure 9), the two resonance peaks merge at 39 kHz resulting in a peak of higher amplitude.

In figure 10 we observe a similar behaviour but in a lower frequency range. In this particular case, the two peaks gradually merge until the current reaches a certain threshold (about 200 mA). Around this threshold, we observed that the two peaks split and have lower amplitude.

3.3. Discussion/analysis

To explain the measured responses, we model the first resonance frequency of the coated cantilever as a function of temperature with a modified expression of the first resonance flexural frequency of a cantilever beam [23]. The basic equation is

$$\omega_0 = \frac{\lambda^2}{2\pi L^2}\sqrt{\frac{E(T)I(T)}{\rho A}} \tag{3.2}$$

with L the length, E the temperature-dependent average Young's modulus of the bimorph cantilever, I the temperature-dependent second moment of area, ρ the density and A the cross-section of the beam. The dimensionless constant λ is the wave number, depending on the boundary conditions for which the resonance frequency is calculated [23]. For a cantilevered beam $\lambda = 1.875\,104\,07$ for the first flexural resonance frequency. As shown in the measurements in section 2.3, as one could expect from the model assumption, the Young's modulus changes during phase transformation (according to figure 4). The bimorph effect resulting from the CTE (coefficient of thermal expansion) mismatch between the SMA film and the silicon causes the curvature of the beam to change not only along its length, but also in the transverse direction (i.e. the anticlastic curvature). Consequently, the second moment of inertia I of the beam changes during the phase transformation. Including this dependence and using the parameters in table 1, we compute the first flexural resonance frequencies as a function of temperature starting from room temperature. The results are shown in figure 11.

From the above figure, we note that the model predicts a frequency shift around 200 mA for the flexural mode calculated around 35.7 kHz (below 200 mA). In the experiments, we indeed found a resonance peak at a frequency of 37 kHz that shifted to a higher level at 200 mA. The calculations show that this mode decreases slightly at low temperatures when the bimorph effect changes the cross-section and thus the second moment of inertia of the beam. We note that the same behaviour is observed experimentally for both cantilevers. After the phase transition from the R-phase to the austenite phase around 60°, Young's modulus of the SMA film increases, resulting in a larger flexural resonance frequency.

For the two cantilevers, there seems to be a good agreement between the model and the experimental observations. We attribute this sharp change of resonant frequency to the R-phase transformation. Indeed, we started our experiments by heating up the cantilever so that the full austenite transformation occurs. The cantilever was then kept at room temperature preventing it from transforming to the martensite phase. We note that experimentally, the measured changes are more dramatic than the model predicts. A possible

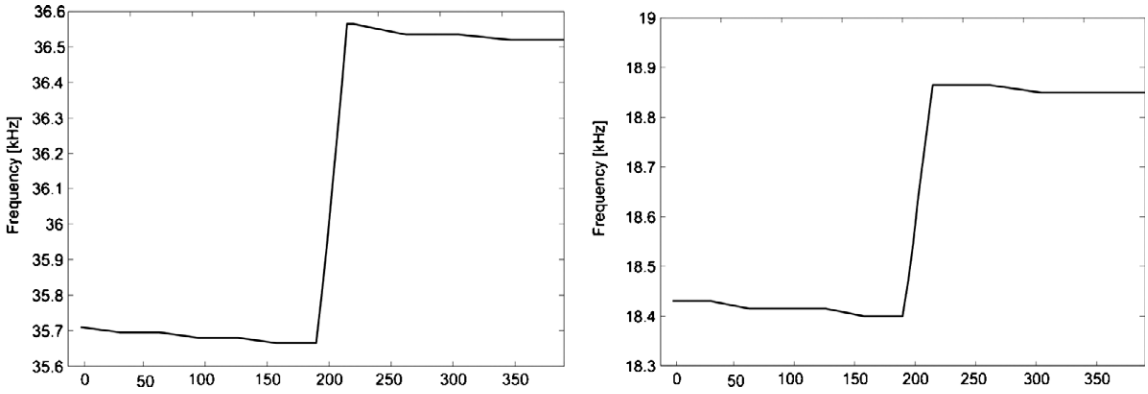

Figure 11. Computed first flexural resonance frequency of the 250 μm (left) and 350 μm cantilever as a function of temperature.

explanation can be in the inaccuracy of the choice of material parameters (for instance with respect to the choice for the Young modulus).

The origin of the second peak and the phenomenon of merging and splitting are not captured by this simple model. Calculations of higher order flexural or torsional resonance frequencies (similar to (3.2)) do not predict the second peak at these locations. As this mode changes slightly as a function of the applied current (and thus temperature), we rule out the possibility of a measurement artefact. Another hypothesis is that this mode is a combined torsional and flexural mode. Note that the low-temperature dependence of this mode indicates that it is less sensitive to the change in flexural stiffness of the beam than the flexural mode. So far, we do not have strong evidence for the combined mode and therefore further work is needed to confirm our hypothesis.

4. Conclusion

In this paper, we have shown that shape memory alloy thin films can effectively be used to modify the dynamic response of atomic force microscope cantilevers. We have measured and interpreted the relation between the applied electrical current in the SMA thin film and the frequency response of the cantilever. This is a first important step towards the goal of implementing close-loop control of cantilevers frequency response that can effectively improve the accuracy (by rejecting unwanted vibrations) and increase the dynamic measurement ranges of such devices.

With our experimental setup, we observed two resonant peaks. While the first peak can be attributed to the flexural mode, the second peak is not predicted by a calculation of higher order flexural or torsional resonance frequencies. We suspect the second resonant peak to originate from a combination of slight bending in the cantilever transverse direction and the natural torsion mode. Interestingly, we observe a separation of the two resonance peaks during the phase transformation.

The applications of this work are multiple. As an illustration and in addition to the possibility to increase the performances of existing micro-cantilever applications (like AFM or mass-spectrometers), the dynamic response tuning can be implemented in tactile applications to modulate individual cantilever vibration amplitudes subjected to a global excitation signal.

From a material sciences investigation point of view, the proposed methodology used in this study provides an interesting platform to investigate shape memory materials properties at the micro-/nano-scale. Specimens with different thin films deposited on it can be rapidly examined and specific material properties like transition temperatures, phase transformation and deposition stresses as well as Young's modulus can be rapidly extracted using a rather simple apparatus. Along these lines, it will be interesting to further explore the effects of certain material parameters such as thin-film texture, film chemistry (that will in particular affect the hysteresis curve and eventually suppress the R-phase) and grain sizes that can be tuned using various heat treatments.

Acknowledgments

We are thankful to Michael Hopper of Quintenz Hybridtechnik in Germany for designing the piezo-amplifier in his spare time, Marc van Maris and Willie ter Elst, both from Eindhoven University of Technology for providing excellent measurement devices in the Multi-Scale Lab and for helping in realizing the experimental setup.

References

[1] Binnig G and Rohrer H 1982 *Helv. Phys. Acta* **55** 726
[2] Ono T and Esashi M 2004 *Meas. Sci. Technol.* **15** 1977–81
[3] Lavrik N V, Sepaniak M J and Datskos P G 2004 *Rev. Sci. Instrum.* **75** 2229–53
[4] Vettiger P *et al* 2002 *IEEE Trans. Nanotechnol.* **1** 39–55
[5] Dolce M, Cardone D and Marnetto R 2000 *Earthq. Eng. Struct. Dyn.* **29** 945–68
[6] Bidaux J-E, Bernet N, Sarva C, Manson J-A E and Gotthardt R 1995 *J. Phys. (France)* IV **5** C8–1177
[7] Scherrer P, Bidaux J E, Kim A, Månson J A E and Gotthardt R 1999 *J. Phys. IV France* **9** 393–400
[8] Otsuka K and Wayman C M 2002 *Shape Memory Materials* (Cambridge: Cambridge University Press)
[9] Bellouard Y and Clavel R 2004 *Mater. Sci. Eng.* A **378** 210–5
[10] Bellouard Y 2008 *Mater. Sci. Eng.* A **481–482** 582–9
[11] Wang X, Rein M and Vlassak J J 2008 *J. Appl. Phys.* **103** 023501
[12] Bekker A and Brinson L C 1998 *Acta Mater.* **46** 3649–65

[13] Boyd J G and Lagoudas D C 1996 *Int. J. Plast.* **12** 805–42
[14] Hughes D and Wen J T 1997 *Smart Mater. Struct.* **6** 287–300
[15] Krasnosel'skii M A and Pokrovskii A V 1989 *Systems with Hysteresis* (Berlin: Springer)
[16] MikroMasch http://www.spmtips.com consulted April 2007
[17] Macki J W, Nistri P and Zecca P 1993 *SIAM Rev.* **35** 94–123
[18] Timoshenko S 1925 *J. Opt. Soc. Am.* **11** 233–55
[19] Wortman J J and Evans R A 1965 *J. Appl. Phys.* **36** 153–6
[20] Wang X 2007 *PhD Thesis* Harvard University, Cambridge, MA, USA
[21] Wang X and Vlassak J J 2009 The effect of film thickness on the martensitic transformation in equi-atomic NiTi thin films constrained by substrates submitted
[22] Wuttig M 2003 *J. Alloys Compd.* **355** 108–12
[23] Volterra E and Zachmanoglou E C 1965 *Dynamics of Vibrations* (Columbus: Charles E. Merrill Books)